Aftershock moment tensor scattering

John Dylan Wilding[1] and Zachary E. Ross[1]

[1]California Institute of Technology

November 26, 2022

Abstract

Coseismic rotations of principal stress axes can provide insights into the strength of the crust, but it is unclear how common this phenomenon is. We use a nearest-neighbor clustering algorithm to identify earthquake sequences in the global ISC-GEM catalog and the regional Southern California catalog. Using an inner-product-based pairwise measure of moment tensor similarity, we demonstrate that, in both catalogs, aftershocks are less similar to their respective mainshocks than foreshocks are. We interpret this effect, which we call moment tensor scattering, as evidence for widespread coseismic stress rotations. Moment tensor scattering is observable for a broad range of mainshock magnitudes in both catalogs. We further demonstrate that mainshock-aftershock similarity recovers logarithmically to pre-mainshock levels on decadal timescales. We conclude that moment tensor scattering is a generally observable feature of seismic sequences which may be useful in future work to discriminate between models of crustal strength.

Aftershock moment tensor scattering

John D. Wilding[1], Zachary E. Ross[1]

[1]Seismological Laboratory, California Institute of Technology, Pasadena, CA, USA

Key Points:

- We examine the similarity of foreshock and aftershock moment tensors relative to mainshocks
- Moment tensors of aftershocks more scattered than those of foreshocks at global and local scales
- Mainshock-aftershock similarity gradually increases in the years following a mainshock

Corresponding author: J. D. Wilding, `jwilding@caltech.edu`

Abstract

Coseismic rotations of principal stress axes can provide insights into the strength of the crust, but it is unclear how common this phenomenon is. We use a nearest-neighbor clustering algorithm to identify earthquake sequences in the global ISC-GEM catalog and the regional Southern California catalog. Using an inner-product-based pairwise measure of moment tensor similarity, we demonstrate that, in both catalogs, aftershocks are less similar to their respective mainshocks than foreshocks are. We interpret this effect, which we call moment tensor scattering, as evidence for widespread coseismic stress rotations. Moment tensor scattering is observable for a broad range of mainshock magnitudes in both catalogs. We further demonstrate that mainshock-aftershock similarity recovers logarithmically to pre-mainshock levels on decadal timescales. We conclude that moment tensor scattering is a generally observable feature of seismic sequences which may be useful in future work to discriminate between models of crustal strength.

Plain Language Summary

Earthquakes can change the stress field in the surrounding crust. One such change is a rotation of the stress tensor's principal axes, which is called coseismic stress rotation. Seismologists can make inferences about the strength of the crust by studying these rotations. However, it is difficult to study coseismic stress rotations systematically because it is unclear if they are a common phenomenon. To study the ubiquity of coseismic stress rotations, we examine both a global earthquake catalog and a local (Southern California) catalog. We calculate the similarity between aftershock and mainshock earthquake mechanisms, and compare this similarity to the similarity between foreshock and mainshock mechanisms. We find that aftershock-mainshock mechanism similarity is significantly reduced with respect to foreshock-mainshock mechanism similarity. This observation is prominent in both the catalogs we study, which we interpret as evidence for widespread coseismic stress rotations. We also find that coseismic stress rotations may linger for decadal timescales after an earthquake occurs. Demonstrating that coseismic stress rotations are a generally observable feature of seismic sequences facilitates our ability to study them systematically. Future studies of coseismic stress rotations will help us to address the question of whether the crust is high-strength or low-strength in seismogenic regions.

1 Introduction

The strength of the crust in seismogenic regions has long been the subject of debate. Laboratory measurements of the frictional strength of fault materials and in situ stress measurements from borehole breakout data have been used to argue the crust is capable of supporting differential stresses on the order of hundreds of MPa (Byerlee, 1978; Zoback & Healy, 1992). Other measurements of fault properties, however, suggest that the true strength of major faults might be reduced from these expectations by an order of magnitude. The so-called heat flow paradox along the San Andreas fault (Brune et al., 1969), in which researchers have identified the absence of a frictional heat flow anomaly and nearly fault-normal maximum compressive stress, has been interpreted as evidence that the crust is weak (Zoback, 2000).

Although the absolute magnitude of stress cannot be measured directly at seismogenic depths, it is still possible to examine how the stress field responds to perturbations caused by earthquakes. Quantitative measurements of the rotation of principal stress axes after earthquakes can provide insight into the strength of the crust and fault mechanics. A common approach to measuring coseismic stress rotations involves the inversion of focal mechanisms for the stress field (e.g. Michael (1987); Hardebeck and Michael (2006); Martínez-Garzón et al. (2016)), which can then be temporally partitioned to study changes induced by large earthquakes. The principal stress axes have been seen to rotate by as

much as 30° close to the mainshock after large earthquakes (Holt et al., 2013; Hardebeck, 2012; Hasegawa et al., 2011). By binning aftershock mechanisms in time, stress rotation studies can also measure the postseismic response of the stress field, which can provide information on postseismic fault processes and the timescale of tectonic reloading. Recent studies have utilized dense arrays and comprehensive seismicity catalogs to show that rebound of the stress field to its pre-mainshock state can be observed over months to years following a large earthquake (e.g., Ickrath et al. (2014); Hardebeck (2012)).

Two competing physical models have been proposed to explain observed stress rotations. The most widely applied framework relates the magnitude of the stress rotation to the size of the earthquake stress drop relative to the background deviatoric stress acting on the fault (Hardebeck & Hauksson, 2001). This model predicts the occurrence of observable stress rotations if the stress drop is roughly the same order of magnitude as the background deviatoric stress. This model has been applied to observations of post-mainshock stress rotations to argue that fault zones are only capable of supporting deviatoric stresses on the order of a typical earthquake stress drop ($\sim 1-10$ MPa) (Hardebeck & Okada, 2018).

Alternatively, it has been proposed that apparent stress rotations measured from aftershock mechanisms are an artifact caused by biased spatial sampling of pre-existing stress heterogeneities (Smith & Dieterich, 2010; Smith & Heaton, 2011). In this model, aftershocks are promoted in patches where the local stress field aligns with stress field changes caused by the mainshock. This biased sampling induces an apparent stress rotation which may be orders of magnitude greater than the true stress change, so that observations of apparent stress rotations are compatible with a strong crust.

Efforts to discriminate between these proposed models are impeded by the unanswered question of whether stress changes are generally observable features of seismicity, or instead occur only under favorable conditions (Hardebeck & Loveless, 2018). Robust observations of coseismic stress changes have been limited to moderate to large earthquakes at subduction zones and along transform boundaries. Hardebeck (2012) examined great subduction zone earthquakes and identified stress rotations for all events with $M \geq 8.7$. Several earthquakes with $M < 8.7$, however, were associated with statistically insignificant or no post-mainshock stress rotations. Although stress rotations have been confirmed for earthquakes as small as magnitude 5.5 near dense seismic arrays (Martínez-Garzón et al., 2016), studies of some larger earthquakes have reported no detectable coseismic stress changes (e.g., Townend and Zoback (2001); Townend et al. (2012); Provost and Houston (2003)). Due to this poor sampling of magnitudes, the ubiquity of coseismic stress rotations, and the magnitude range at which they may be observed, have not been systematically constrained. Providing additional evidence for ubiquitous, detectable coseismic stress changes would increase the number of candidate earthquakes for studying these stress changes.

In this study, our contributions are as follows. We quantitatively assess the similarity between aftershocks and their corresponding mainshocks to investigate the general observability of coseismic stress changes at local and global scales. These mechanism similarity data can be statistically compared with similarity between foreshocks and mainshocks. Increased dissimilarity between mainshocks and aftershocks relative to the foreshock-mainshock baseline would provide evidence for detectable stress changes in the wake of mainshocks.

2 Methods

2.1 Seismicity catalogs

Our analysis is focused on aspects of moment tensors at both global and regional scales, and thus we work with catalogs of moment tensors. For the global scale, we an-

alyze the ISC-GEM Global Instrumental Earthquake Catalogue with Global Centroid Moment Tensor (GCMT) solutions attached (D. A. Storchak et al., 2013; D. Storchak et al., 2015; Di Giacomo et al., 2018; Bondár et al., 2015; Dziewonski et al., 1981; Ekström et al., 2012). We work only with events in the catalog that occurred after 1976, since this is the start date of the GCMT catalog. Presently, the GEM catalog is complete through 2017. The catalog is filtered with a lower cutoff magnitude of 5.45, and only events with reported GCMT solutions are retained for analysis. Although it is possible that some low-magnitude events were not captured due to limited Global Seismographic Network coverage in the early years of GCMT operation, the clustering methodology which we use to identify foreshock-mainshock-aftershock sequences has been demonstrated to be robust to magnitude incompleteness (Zaliapin & Ben-Zion, 2013). The final catalog contains 17,096 events.

We also analyze the waveform cross-correlation relocated seismicity catalog for Southern California (Hauksson et al., 2012; Lin et al., 2007) in order to complement our global analysis with a high-quality catalog which includes smaller, local events. Based on the conclusions of Hutton et al. (2010), we select 1.8 as the completeness magnitude (M_c), resulting in 185,805 events for the period 1981-2019. We then associate events in our catalog with focal mechanisms reported by Yang et al. (2012).

2.2 Cluster analysis

Our study is focused on analyzing the behavior of earthquake clusters. To identify sequences of clustered seismicity, we use the nearest-neighbor-distance method of Zaliapin and Ben-Zion (2013) (NND), which makes relatively minimal assumptions about the statistical properties of seismicity. We apply the same clustering methodology to both catalogs, and describe the general approach below.

The NND method involves (i) computing a space-time distance between all pairs of events in the catalog, (ii) constructing a large directed acyclic tree, and (iii) breaking the links when the NND exceeds some threshold. This provides a straightforward approach to grouping events into clusters. The method has previously been applied to both of the catalogs we use and shown to work effectively. Here, we apply the method to these catalogs without modification, using the parameters described in Zaliapin and Ben-Zion (2013) and Zaliapin and Ben-Zion (2016). Following Zaliapin and Ben-Zion (2013), we use a Gaussian mixture model to determine the optimal threshold for breaking the links from the data.

To quantify the similarity between two moment tensors, M^1 and M^2, we use the cosine similarity, $r \in [-1, 1]$, defined as

$$r = \frac{\sum_i \sum_j M_{ij}^1 M_{ij}^2}{\|M^1\| \|M^2\|}. \tag{1}$$

Here, $\|\cdot\|$ denotes the Euclidean norm. This operation is an extension of the normalized dot product to tensors and has been previously used to compare stress tensors (Hardebeck, 2014). A value of $r = -1$ indicates antisimilarity, $r = 0$ indicates orthogonality, and $r = 1$ indicates that the tensors are geometrically identical. Intermediate values indicate some degree of rotation or, in the case of the global catalog, differential non-double-couple contributions between a pair of moment tensors.

We use the cosine similarity metric to include not only rotations of double-couple components but differences in non-double-couple moment tensor components in our analysis. In order to make use of the same similarity metric for both the ISC-GEM and SCSN catalogs, we convert SCSN focal mechanism parameters to moment tensors to compute pairwise similarity values. While moment tensors associated with the SCSN catalog are entirely double-couple by construction, having been converted from focal mechanism pa-

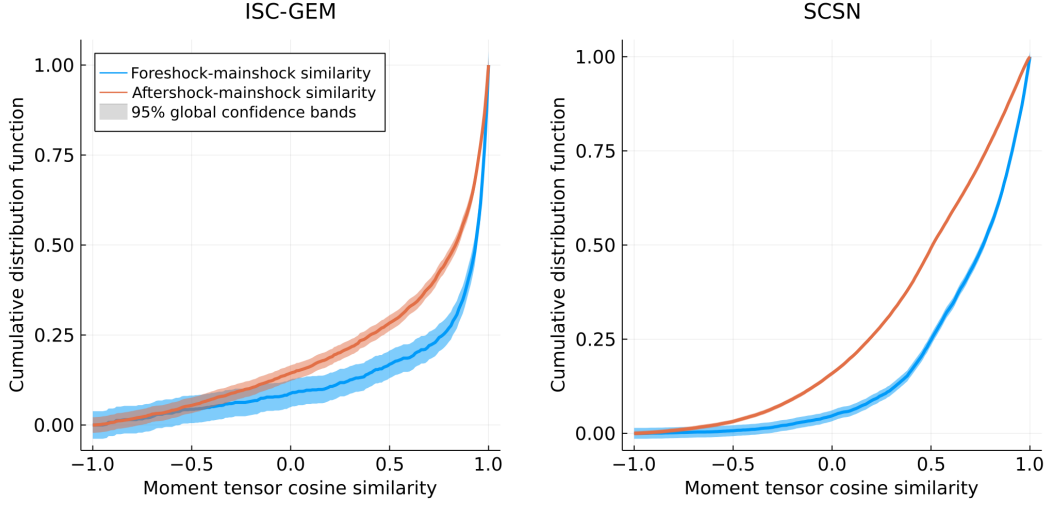rameters, we retain the full the moment tensor solutions reported by the GCMT catalog.

3 Results

The NND clustering algorithm sorts each catalog into discrete clusters of events (sequences), resulting in 12,265 clusters for the global catalog and and 112,186 clusters for the SCSN catalog. Of these clusters, 10,472 in the ISC-GEM catalog and 48,713 in the SCSN catalog are classified by the algorithm as so-called "singles" which are clustered with no other event in the catalog. We discard these events to study sequences composed of more than one earthquake, resulting in 1,793 sequences for the ISC-GEM catalog and 11,122 sequences for the SCSN catalog. Following Zaliapin and Ben-Zion (2013), we classify the highest-magnitude event within a sequence as the mainshock; events within the sequence that precede the mainshock are classified as foreshocks, and events in the sequence that occur after the mainshock are classified as aftershocks. Within the ISC-GEM catalog, we identify 942 foreshocks, 1,793 mainshocks, and 3,889 aftershocks. Similarly for the SCSN catalog, we obtain 7,521 foreshocks, 26,968 mainshocks, and 55,667 aftershocks after filtering to remove events for which no focal mechanism parameters are reported by Yang et al. (2012).
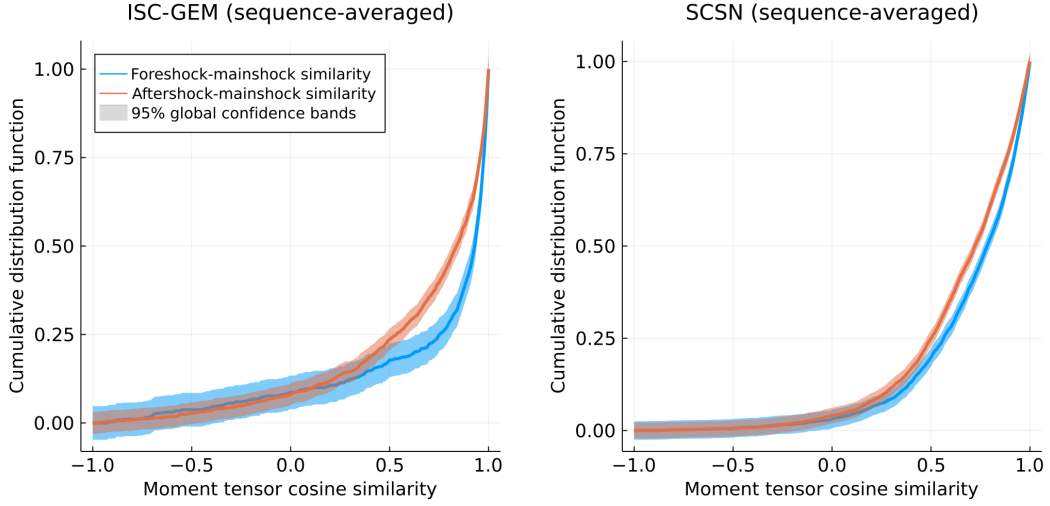
For both catalogs, we calculate r values for all foreshock-mainshock pairs and aftershock-mainshock pairs, which generates two distributions which we refer to as r_F and r_A, respectively. These distributions contain information about the source mechanism similarity of foreshock-mainshock pairs and aftershock-mainshock pairs stacked over all sequences in a catalog. Pairwise moment tensor similarity values are not calculated for foreshock-mainshock or mainshock-aftershock pairs in the SCSN catalog whenever one event is missing focal mechanism information. We then compare the r_F and r_A distributions for both catalogs (represented as cumulative distribution functions in Fig. 1) to identify evidence of lower r_A values relative to r_F. We calculate 95% global confidence bands on the CDFs through bootstrapping (Loh, 2008). Both r_F and r_A distributions are concentrated near the maximum value of 1.0, indicating that, within both catalogs, mechanisms of foreshocks and aftershocks are generally similar to those of their corresponding mainshocks. We additionally find that, for both catalogs, r_A tends to be significantly lower than r_F. For the ISC-GEM catalog, the mean values of r_F and r_A are 0.742 and 0.600, respectively. For the SCSN catalog, the mean values of r_F and r_A are respectively 0.666 and 0.437. We refer to this heightened dissimilarity between mainshock and aftershock mechanisms as moment tensor scattering. We interpret this ubiquitous mainshock-aftershock dissimilarity as resulting from widespread mainshock-induced changes to the local stress field (coseismic stress rotations).

We note that this pairwise analysis is naturally biased towards large magnitude earthquakes with productive aftershock sequences. A small number of sequences in each catalog are comprised of a significantly larger number of events than the other sequences. In the SCSN catalog, aftershocks associated with the $M_W 7.3$ Landers and $M_W 7.2$ El Mayor - Cucapah earthquakes account for 31.7% of the total number of aftershocks in the catalog. Similarly, in the ISC-GEM catalog, $M_W \geq 8$ events account for only 1.6% of mainshocks with aftershocks, but these events produce 21.1% of the observed aftershocks. Because of this natural bias, it is difficult to conclude from this analysis alone whether the observed moment tensor scattering signal is the result of scattering over the entire catalog or whether it is produced by a small handful of large-magnitude earthquakes.

An alternative way to examine moment tensor similarity is by giving more weight to the smaller sequences, which highlights different, but complementary, components of the data. We can compute weighted versions of r_F and r_A by weighting each observation inversely by the number of foreshocks and aftershocks in that sequence. We calculate a single mean value of r_F and r_A for every sequence which has foreshocks or after-
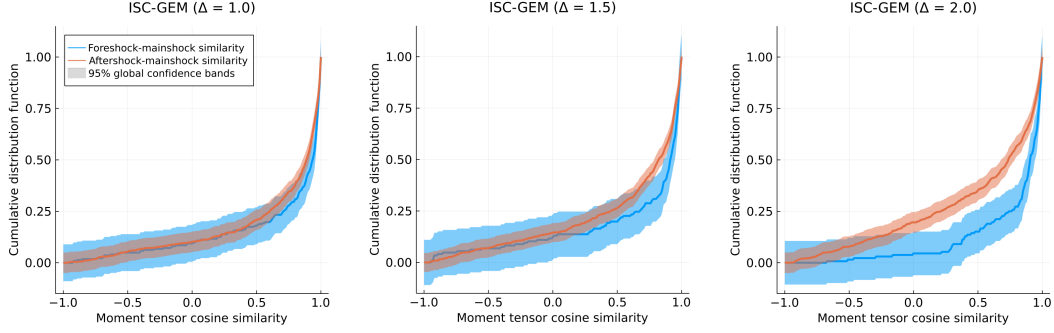
Figure 1. Cumulative distribution functions of r_F and r_A calculated with (left) the ISC-GEM catalog and (right) the SCSN catalog. Note that r_A values are overall lower than r_F values.

Figure 2. Cumulative distribution functions of sequence-averaged r_F and r_A distributions calculated over sequences from (left) the ISC-GEM catalog and (right) the SCSN catalog.

shocks, respectively. These values form new r_F and r_A distributions which we refer to as sequence-averaged (Fig. 2). Within these sequence-averaged r distributions, sequences of any length are represented by a single value in r_F and r_A, so that these distributions are biased towards short foreshock and aftershock sequences (which account for the majority of sequences in both catalogs).

For both catalogs, we observe that the sequence-averaged r_F and r_A distributions are separated, indicating that moment tensor scattering is observable for many sequences in each catalog and not exclusively for sequences with high mainshock magnitude M_M. However, the difference between the r_F and r_A distributions is reduced in this analysis relative to the previous pairwise analysis. This effect is particularly prominent for the SCSN catalog. While the difference between sequence-averaged r_F and r_A for the SCSN catalog is statistically significant according to our global confidence bands, the magni-

Figure 3. Cumulative distribution functions of r_F and r_A calculated for the ISC-GEM catalog using Δ-analyses. Moment tensor scattering is negligible for $\Delta = 1.0$, but statistically significant separation of the foreshock-mainshock and aftershock-mainshock similarity distributions is visible for analyses with $\Delta \geq 1.5$.
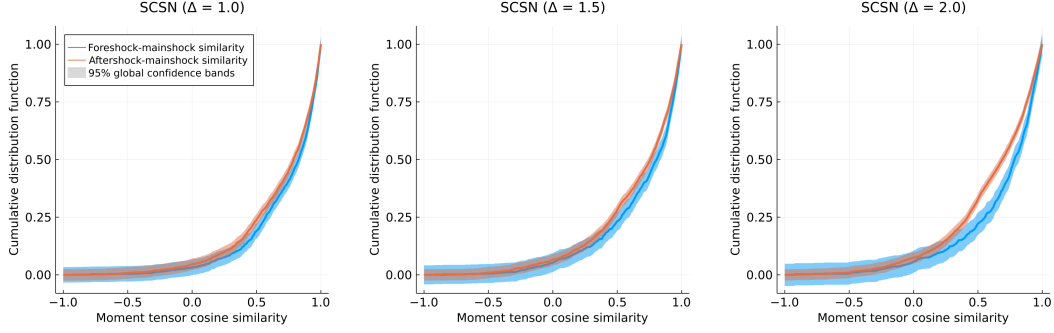
tude of the difference between the distributions is minimal. The weighting scheme we have introduced deweights contributions to the distributions from higher magnitude mainshocks, which are farther from the catalog's magnitude of completeness and are thus more likely to have productive aftershock sequences. The corresponding reduction in the magnitude of moment tensor scattering indicates that moment tensor scattering is more easily observed for sequences with large mainshocks relative to M_C, or equivalently, earthquake sequences with higher $M_M - M_A$ values (where M_A denotes aftershock magnitude).

Understanding the degree to which the $\Delta = M_M - M_A$ value affects the observability of moment tensor scattering has important implications for stress rotation studies. For example, if moment tensor scattering is only significant for mainshock-aftershock pairs with large differences in magnitude, stress rotations will not be detectable for earthquakes with a magnitude close to the magnitude of completeness. In order to quantify the control of Δ values on the detectability of moment tensor scattering, we perform a series of so-called Δ-analyses (e.g. Zaliapin and Ben-Zion (2013)), wherein we recalculate r_A and r_F including only: (i) mainshocks with $M > M_C + \Delta$, and (ii) foreshocks and aftershocks with $M > M_M - \Delta$.

We calculate pairwise foreshock and aftershock similarity distributions by computing and stacking mainshock similarity values for all foreshock-mainshock and aftershock-mainshock pairs which meet the above criteria. This analysis allows us to test the observability of moment tensor scattering for sequences with small Δ values. Results for both catalogs for $\Delta = 1.0$, 1.5, and 2.0 are reported in Figs. 3 and 4.

For both catalogs, r_F and r_A grow progressively more differentiated with increasing Δ values. A statistically significant differentiation of the distributions can be observed for $\Delta_{ISC} \geq 1.5$ for the ISC-GEM catalog and $\Delta_{SCSN} \geq 2.0$ for the SCSN catalog. These values indicate that moment tensor scattering is observable even for mainshock-aftershock pairs with relatively small differences in magnitude. This observation suggests that moment tensor scattering may be measurable even for events which have magnitudes which are relatively close to the magnitude of completeness. We identify this observation as evidence for moment tensor scattering being a pervasive characteristic of seismicity which is observable across a wide range of magnitudes at local and global scales.
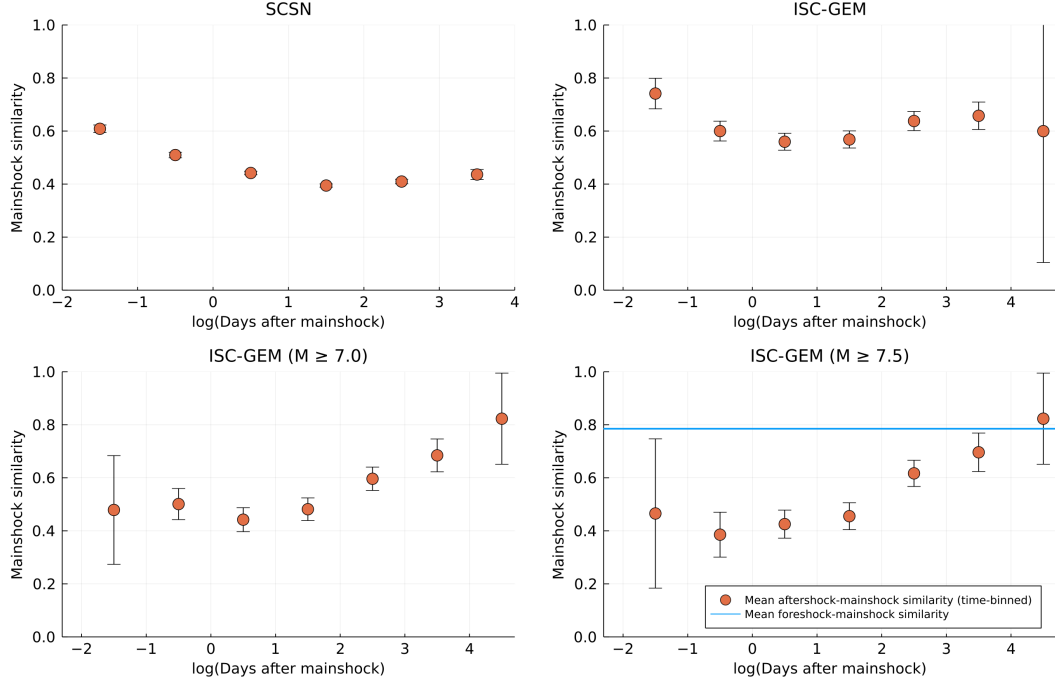
Figure 4. Same as Fig. 3, but for the SCSN catalog. Statistically significant separation between r_F and r_A emerges at $\Delta = 2.0$.

3.1 Temporal analysis

Given that we are studying the similarity of aftershock focal mechanisms with respect to the mainshock, it is natural to wonder if our observations of moment tensor scattering vary with the time elapsed since the mainshock. To investigate, we bin aftershocks by the logarithm of time elapsed since the mainshock and calculate r_A within these bins. Our selected bins for the ISC-GEM catalog span the range [-2, 5] logarithmic days elapsed since the mainshock, with a bin width of one logarithmic unit. For the SCSN catalog, we use bins spanning the range [-3, 4] logarithmic days with a bin width of one logarithmic unit. Within each bin, we calculate the mean of r_A and estimate uncertainty as 2 · standard error. We find that no monotonic trend in time is evident for the ISC-GEM and SCSN catalogs (Fig. 5). Motivated by our previous observation that moment tensor scattering is more easily observable for higher magnitude mainshocks, we focus our analysis on the ISC-GEM catalog and introduce a lower M_M cutoff to our calculations of foreshock and aftershock similarity distributions, excluding sequences for which M_M is below this cutoff. We progressively increase this cutoff value, at each step examining the variability of aftershock values in time. For a lower M_M cutoff of $M_W 7.0$, we observe that average time-binned r_A values increase with logarithmic time beginning 10 days after the mainshock. When the lower M_M cutoff is increased to $M_W 7.5$, this temporal trend becomes more significant (Fig. 5). We observe that mean aftershock similarity is lowest during the one-day period following the mainshock. A significant and monotonic rebound in aftershock similarity commences after one day and continues to be observable to 10^4 days (27.4 years) post-mainshock, which is comparable to the duration of the entire catalog. At 10^4 days post-mainshock, mean aftershock similarity values roughly correspond to the mean pre-mainshock foreshock similarity value for sequences with $M_M \geq 7.5$ (0.785). The apparent longevity of the stress field's response to large earthquakes suggests that these earthquakes induce detectable alterations to the regional stress field that may persist on decadal timescales.

For each increase of the lower M_M cutoff value, we repeat the time-binning analysis on r_F values to search for evidence of temporal variability of foreshock-mainshock similarity. We find that foreshock similarity values, in contrast to aftershock similarity values, display no temporal dependence. This observation is consistent with our interpretation of foreshock-mainshock similarity as a proxy for a relatively stable state of pre-mainshock stress which is then altered during mainshocks.

Figure 5. Top left: mean values of aftershock similarity for the SCSN catalog binned by time since the mainshock. Top right: time-binned mean values of aftershock similarity for the ISC-GEM catalog. Bottom left: time-binned mean values of aftershock similarity for the ISC-GEM catalog with a minimum mainshock magnitude cutoff of 7.0. Bottom right: time-binned mean values of aftershock similarity for the ISC-GEM catalog with a minimum mainshock magnitude cutoff of 7.0. The mean value of foreshock similarity for sequences included in this plot, which is stationary in time, is shown in blue. For all mean values plotted, error bars are estimated as $2 \cdot$ standard error.

4 Discussion

Coseismic stress rotations are usually identified by inverting for a pre-mainshock and a post-mainshock state of stress. These stress tensor inversions require manual spatial and temporal binning, and rely upon the availability of both foreshock and aftershock mechanisms (Michael, 1987). Additionally, accounting for focal mechanism uncertainty and the natural variability of focal mechanisms within sequences, stress rotations must exceed an uncertainty threshold of up to 10° (Hardebeck & Okada, 2018). Previous studies have successfully identified post-mainshock stress heterogeneities by directly comparing aftershock source mechanisms (Beroza & Zoback, 1993). Trugman et al. (2020) analyzed focal mechanism similarity between aftershocks of the Ridgecrest sequence using the Kagan angle measure, demonstrating that mechanism similarity between neighboring aftershocks drops significantly post-mainshock and interpreting this observation as evidence for a heterogenous state of stress near the rupture area. Using direct comparisons of seismic sources to search for apparent stress changes after earthquakes avoids the uncertainty and nonuniqueness associated with inversions for the stress state (Hardebeck & Okada, 2018).

By stacking observations of foreshock-mainshock similarity and aftershock-mainshock similarity from multiple sequences within the ISC-GEM and SCSN catalogs, we show that moment tensors of aftershocks tend to be more scattered, or less similar to the mainshock than foreshocks. Examining both the local and global catalogs together, we conclude that moment tensor scattering is observable on both scales. We also demonstrate that moment tensor scattering is observable for mainshock-aftershock pairs with small values of Δ. We interpret this phenomenon as evidence for the general ubiquity of coseismic stress rotations, resulting in aftershock mechanisms which are, on average, less aligned with the mainshock than pre-mainshock earthquake mechanisms. Although our stacking approach allows us to identify moment tensor scattering as a general feature of our catalogs, this technique does not allow us to quantify the degree of stress rotation for individual sequences.

The demonstrated generality of moment tensor scattering greatly expands the potential for observations of coseismic stress rotations in the lithosphere, which will enable enhanced study of the stress rotation phenomenon in the future. The prevalence of moment tensor scattering for sequences with small Δ values suggests that stress rotations may be expected even for earthquakes which are close to a catalog's magnitude of completeness. Where available, high-quality regional focal mechanism catalogs may be used to systematically analyze apparent stress rotations. This prospect mitigates what has been a major obstacle in the study of these stress changes, and will enable further testing of the proposed models of coseismic stress changes, with important implications for interpreting the strength of faults.

Temporal analysis of aftershock similarity suggests that the stress field in the lithosphere may continue to rebound from perturbations caused by large ($M_W \geq 7.5$) earthquakes over decadal timescales. Existing observations of the longevity of apparent stress changes from individual earthquakes are highly variable; most studies identify a near-complete stress field recovery on the scale of months to years (e.g., Ickrath et al. (2014); Hauksson (1994); Zhao et al. (1997)), although some studies measure much slower recovery times, or are unable to resolve temporal recovery at all (Hardebeck & Okada, 2018). The average rate of aftershock similarity rebound recovered in our study probably represents a summed contribution from multiple processes occurring at different timescales. Our observation that the stress field continues to respond to large mainshocks up to 10^4 days post-mainshock suggests that variability in the apparent stress field could result from tectonic reloading, the activation of long-lived fault processes, or a viscoelastic response in the mantle. We also observe that aftershock similarity rebound is more readily observed for higher magnitude earthquakes. By selecting for higher magnitudes, we bias our mainshock selection to include a greater proportion of subduction zone sequences.

Thus, the observed magnitude dependence might reflect a contribution of mantle processes to the timescale of aftershock similarity rebound, although the ISC-GEM catalog contains too few large non-subduction zone mainshocks to formally test this idea.

5 Open Research

The ISC-GEM catalog (D. A. Storchak et al., 2013; D. Storchak et al., 2015; Di Giacomo et al., 2018; Bondár et al., 2015) is available for download at `https://www.isc.ac.uk/iscgem/`. GCMT solutions (Dziewonski et al., 1981; Ekström et al., 2012) are available for download at `https://globalcmt.org`. Southern California data products are from the Southern California Seismic Network and Southern California Earthquake Data Center (doi:10.7909/C3WD3xH1). The waveform cross-correlation relocated SCSN catalog (Hauksson et al., 2012; Lin et al., 2007) and focal mechanism data for this catalog (Yang et al., 2012) are available for download at `https://scedc.caltech.edu/data/downloads.html`.

References

Beroza, G. C., & Zoback, M. D. (1993, January). Mechanism Diversity of the Loma Prieta Aftershocks and the Mechanics of Mainshock-Aftershock Interaction. *Science*, *259*(5092), 210–213. Retrieved 2022-02-22, from `https://www.science.org/doi/10.1126/science.259.5092.210` doi: 10.1126/science.259.5092.210

Bondár, I., Engdahl, E. R., Villaseñor, A., Harris, J., & Storchak, D. (2015, February). ISC-GEM: Global Instrumental Earthquake Catalogue (1900–2009), II. Location and seismicity patterns. *Physics of the Earth and Planetary Interiors*, *239*, 2–13. Retrieved 2022-02-22, from `https://linkinghub.elsevier.com/retrieve/pii/S0031920114001472` doi: 10.1016/j.pepi.2014.06.002

Brune, J. N., Henyey, T. L., & Roy, R. F. (1969, July). Heat flow, stress, and rate of slip along the San Andreas Fault, California. *Journal of Geophysical Research*, *74*(15), 3821–3827. Retrieved 2022-02-22, from `http://doi.wiley.com/10.1029/JB074i015p03821` doi: 10.1029/JB074i015p03821

Byerlee, J. (1978). Friction of Rocks. In J. D. Byerlee & M. Wyss (Eds.), *Rock Friction and Earthquake Prediction* (pp. 615–626). Basel: Birkhäuser Basel. Retrieved 2022-02-22, from `http://link.springer.com/10.1007/978-3-0348-7182-2_4` doi: 10.1007/978-3-0348-7182-2_4

Di Giacomo, D., Engdahl, E. R., & Storchak, D. A. (2018, October). The ISC-GEM Earthquake Catalogue (1904–2014): status after the Extension Project. *Earth System Science Data*, *10*(4), 1877–1899. Retrieved 2022-02-22, from `https://essd.copernicus.org/articles/10/1877/2018/` doi: 10.5194/essd-10-1877-2018

Dziewonski, A. M., Chou, T.-A., & Woodhouse, J. H. (1981, April). Determination of earthquake source parameters from waveform data for studies of global and regional seismicity. *Journal of Geophysical Research: Solid Earth*, *86*(B4), 2825–2852. Retrieved 2022-02-22, from `http://doi.wiley.com/10.1029/JB086iB04p02825` doi: 10.1029/JB086iB04p02825

Ekström, G., Nettles, M., & Dziewoński, A. (2012, June). The global CMT project 2004–2010: Centroid-moment tensors for 13,017 earthquakes. *Physics of the Earth and Planetary Interiors*, *200-201*, 1–9. Retrieved 2022-02-22, from `https://linkinghub.elsevier.com/retrieve/pii/S0031920112000696` doi: 10.1016/j.pepi.2012.04.002

Hardebeck, J. L. (2012). Coseismic and postseismic stress rotations due to great subduction zone earthquakes. *Geophysical Research Letters*, *39*(21). Retrieved 2021-09-21, from `https://onlinelibrary.wiley.com/doi/abs/10.1029/2012GL053438` (_eprint:

https://agupubs.onlinelibrary.wiley.com/doi/pdf/10.1029/2012GL053438)   doi:
10.1029/2012GL053438

Hardebeck, J. L.   (2014).   The impact of static stress change, dy-
namic stress change, and the background stress on aftershock fo-
cal mechanisms.   *Journal of Geophysical Research: Solid Earth*,
119(11), 8239–8266.   Retrieved 2021-10-14, from `https://`
`onlinelibrary.wiley.com/doi/abs/10.1002/2014JB011533`   (_eprint:
https://agupubs.onlinelibrary.wiley.com/doi/pdf/10.1002/2014JB011533)   doi:
10.1002/2014JB011533

Hardebeck, J. L., & Hauksson, E. (2001). Crustal stress field in southern California
and its implications for fault mechanics.   *Journal of Geophysical Research:*
Solid Earth, *106*(B10), 21859–21882.   Retrieved 2021-09-21, from `https://`
`onlinelibrary.wiley.com/doi/abs/10.1029/2001JB000292`   (_eprint:
https://agupubs.onlinelibrary.wiley.com/doi/pdf/10.1029/2001JB000292)   doi:
10.1029/2001JB000292

Hardebeck, J. L., & Loveless, J. P.   (2018, January).   Creeping subduction zones
are weaker than locked subduction zones.   *Nature Geoscience*, *11*(1), 60–
64.   Retrieved 2021-10-14, from `https://www.nature.com/articles/`
`s41561-017-0032-1`   (Bandiera_abtest: a Cg_type: Nature Research Jour-
nals Number: 1 Primary_atype: Research Publisher: Nature Publishing Group
Subject_term: Natural hazards;Solid Earth sciences;Tectonics Subject_term_id:
natural-hazards;solid-earth-sciences;tectonics) doi: 10.1038/s41561-017-0032-1

Hardebeck, J. L., & Michael, A. J.   (2006, November).   Damped regional-scale
stress inversions: Methodology and examples for southern California and
the Coalinga aftershock sequence: DAMPED REGIONAL-SCALE STRESS
INVERSIONS.   *Journal of Geophysical Research: Solid Earth*, *111*(B11),
n/a–n/a.   Retrieved 2022-02-22, from `http://doi.wiley.com/10.1029/`
`2005JB004144`   doi: 10.1029/2005JB004144

Hardebeck, J. L., & Okada, T.   (2018).   Temporal Stress Changes Caused
by Earthquakes: A Review.   *Journal of Geophysical Research: Solid*
Earth, *123*(2), 1350–1365.   Retrieved 2021-09-19, from `https://`
`onlinelibrary.wiley.com/doi/abs/10.1002/2017JB014617`   (_eprint:
https://agupubs.onlinelibrary.wiley.com/doi/pdf/10.1002/2017JB014617)   doi:
10.1002/2017JB014617

Hasegawa, A., Yoshida, K., & Okada, T.   (2011, September).   Nearly com-
plete stress drop in the 2011 Mw 9.0 off the Pacific coast of Tohoku Earth-
quake.   *Earth, Planets and Space*, *63*(7), 35.   Retrieved 2021-10-13, from
`https://doi.org/10.5047/eps.2011.06.007`   doi: 10.5047/eps.2011.06.007

Hauksson, E.   (1994, June).   State of stress from focal mechanisms before and af-
ter the 1992 landers earthquake sequence. *Bulletin of the Seismological Society*
of America, *84*(3), 917–934. Retrieved 2021-09-21, from `https://doi.org/10`
`.1785/BSSA0840030917`   doi: 10.1785/BSSA0840030917

Hauksson, E., Yang, W., & Shearer, P. M.   (2012, October).   Waveform Relocated
Earthquake Catalog for Southern California (1981 to June 2011).   *Bulletin of*
the Seismological Society of America, *102*(5), 2239–2244. Retrieved 2022-01-24,
from `https://doi.org/10.1785/0120120010`   doi: 10.1785/0120120010

Holt, R., Savage, M., Townend, J., Syracuse, E., & Thurber, C.   (2013, Decem-
ber). Crustal stress and fault strength in the Canterbury Plains, New Zealand.
Earth and Planetary Science Letters, *383*, 173–181. Retrieved 2022-02-22, from
`https://linkinghub.elsevier.com/retrieve/pii/S0012821X13005529`
doi: 10.1016/j.epsl.2013.09.041

Hutton, K., Woessner, J., & Hauksson, E.   (2010, April).   Earthquake Monitoring
in Southern California for Seventy-Seven Years (1932-2008).   *Bulletin of the*
Seismological Society of America, *100*(2), 423–446. Retrieved 2022-02-22, from
`https://pubs.geoscienceworld.org/bssa/article/100/2/423-446/349275`

445 doi: 10.1785/0120090130

446 Ickrath, M., Bohnhoff, M., Bulut, F., & Dresen, G. (2014, February). Stress rota-
447   tion and recovery in conjunction with the 1999 Izmit Mw 7.4 earthquake. *Geo-*
448   *physical Journal International*, *196*(2), 951–956. Retrieved 2021-09-21, from
449   `https://doi.org/10.1093/gji/ggt409` doi: 10.1093/gji/ggt409

450 Lin, G., Shearer, P. M., & Hauksson, E. (2007, December). Applying a three-
451   dimensional velocity model, waveform cross correlation, and cluster analysis
452   to locate southern California seismicity from 1981 to 2005. *Journal of Geo-*
453   *physical Research*, *112*(B12), B12309. Retrieved 2022-02-22, from `http://`
454   `doi.wiley.com/10.1029/2007JB004986` doi: 10.1029/2007JB004986

455 Loh, J. M. (2008, July). A Valid and Fast Spatial Bootstrap for Correlation Func-
456   tions. *The Astrophysical Journal*, *681*(1), 726–734. Retrieved 2022-02-23,
457   from `https://iopscience.iop.org/article/10.1086/588631` doi: 10.1086/
458   588631

459 Martínez-Garzón, P., Ben-Zion, Y., Abolfathian, N., Kwiatek, G., & Bohnhoff, M.
460   (2016, December). A refined methodology for stress inversions of earthquake
461   focal mechanisms. *Journal of Geophysical Research: Solid Earth*, *121*(12),
462   8666–8687. Retrieved 2022-02-22, from `https://onlinelibrary.wiley.com/`
463   `doi/10.1002/2016JB013493` doi: 10.1002/2016JB013493

464 Michael, A. J. (1987). Stress rotation during the Coalinga Aftershock
465   Sequence. *Journal of Geophysical Research: Solid Earth*, *92*(B8),
466   7963–7979. Retrieved 2021-09-21, from `https://onlinelibrary`
467   `.wiley.com/doi/abs/10.1029/JB092iB08p07963` (_eprint:
468   https://agupubs.onlinelibrary.wiley.com/doi/pdf/10.1029/JB092iB08p07963)
469   doi: 10.1029/JB092iB08p07963

470 Provost, A.-S., & Houston, H. (2003, October). Investigation of temporal varia-
471   tions in stress orientations before and after four major earthquakes in Cal-
472   ifornia. *Physics of the Earth and Planetary Interiors*, *139*(3-4), 255–267.
473   Retrieved 2022-02-22, from `https://linkinghub.elsevier.com/retrieve/`
474   `pii/S0031920103001924` doi: 10.1016/j.pepi.2003.09.007

475 Smith, D. E., & Dieterich, J. H. (2010). Aftershock Sequences Modeled with 3-D
476   Stress Heterogeneity and Rate-State Seismicity Equations: Implications for
477   Crustal Stress Estimation. In M. K. Savage, D. A. Rhoades, E. G. C. Smith,
478   M. C. Gerstenberger, & D. Vere-Jones (Eds.), *Seismogenesis and Earthquake*
479   *Forecasting: The Frank Evison Volume II* (pp. 213–231). Basel: Springer. Re-
480   trieved 2021-09-19, from `https://doi.org/10.1007/978-3-0346-0500-7_14`
481   doi: 10.1007/978-3-0346-0500-7_14

482 Smith, D. E., & Heaton, T. H. (2011, June). Models of Stochastic, Spatially Varying
483   Stress in the Crust Compatible with Focal-Mechanism Data, and How Stress
484   Inversions Can Be Biased toward the Stress Rate. *Bulletin of the Seismo-*
485   *logical Society of America*, *101*(3), 1396–1421. Retrieved 2021-09-19, from
486   `https://doi.org/10.1785/0120100058` doi: 10.1785/0120100058

487 Storchak, D., Di Giacomo, D., Engdahl, E., Harris, J., Bondár, I., Lee, W.,
488   . . . Villaseñor, A. (2015, February). The ISC-GEM Global Instrumen-
489   tal Earthquake Catalogue (1900–2009): Introduction. *Physics of the*
490   *Earth and Planetary Interiors*, *239*, 48–63. Retrieved 2022-02-22, from
491   `https://linkinghub.elsevier.com/retrieve/pii/S003192011400154X`
492   doi: 10.1016/j.pepi.2014.06.009

493 Storchak, D. A., Di Giacomo, D., Bondar, I., Engdahl, E. R., Harris, J., Lee,
494   W. H. K., . . . Bormann, P. (2013, September). Public Release of the
495   ISC-GEM Global Instrumental Earthquake Catalogue (1900-2009). *Seis-*
496   *mological Research Letters*, *84*(5), 810–815. Retrieved 2022-02-22, from
497   `https://pubs.geoscienceworld.org/srl/article/84/5/810-815/315315`
498   doi: 10.1785/0220130034

499 Townend, J., Sherburn, S., Arnold, R., Boese, C., & Woods, L. (2012, Novem-

ber).   Three-dimensional variations in present-day tectonic stress along the Australia–Pacific plate boundary in New Zealand.   *Earth and Planetary Science Letters*, *353-354*, 47–59.   Retrieved 2022-02-22, from `https://linkinghub.elsevier.com/retrieve/pii/S0012821X1200430X`   doi: 10.1016/j.epsl.2012.08.003

Townend, J., & Zoback, M. D.   (2001).   Implications of earthquake focal mechanisms for the frictional strength of the San Andreas fault system.   *Geological Society, London, Special Publications*, *186*(1), 13–21.   Retrieved 2022-02-22, from `http://sp.lyellcollection.org/lookup/doi/10.1144/GSL.SP.2001.186.01.02`   doi: 10.1144/GSL.SP.2001.186.01.02

Trugman, D. T., Ross, Z. E., & Johnson, P. A.   (2020).   Imaging Stress and Faulting Complexity Through Earthquake Waveform Similarity.   *Geophysical Research Letters*, *47*(1), e2019GL085888.   Retrieved 2021-10-14, from `https://onlinelibrary.wiley.com/doi/abs/10.1029/2019GL085888`   (_eprint: https://agupubs.onlinelibrary.wiley.com/doi/pdf/10.1029/2019GL085888)   doi: 10.1029/2019GL085888

Yang, W., Hauksson, E., & Shearer, P. M.   (2012, June).   Computing a Large Refined Catalog of Focal Mechanisms for Southern California (1981-2010): Temporal Stability of the Style of Faulting.   *Bulletin of the Seismological Society of America*, *102*(3), 1179–1194.   Retrieved 2022-02-22, from `https://pubs.geoscienceworld.org/bssa/article/102/3/1179-1194/349692`   doi: 10.1785/0120110311

Zaliapin, I., & Ben-Zion, Y.   (2016, October).   A global classification and characterization of earthquake clusters.   *Geophysical Journal International*, *207*(1), 608–634.   Retrieved 2022-02-22, from `https://academic.oup.com/gji/article-lookup/doi/10.1093/gji/ggw300`   doi: 10.1093/gji/ggw300

Zaliapin, I., & Ben-Zion, Y.   (2013).   Earthquake clusters in southern California I: Identification and stability.   *Journal of Geophysical Research: Solid Earth*, *118*(6), 2847–2864.   Retrieved 2021-01-19, from `https://agupubs.onlinelibrary.wiley.com/doi/abs/10.1002/jgrb.50179`   (_eprint: https://agupubs.onlinelibrary.wiley.com/doi/pdf/10.1002/jgrb.50179)   doi: https://doi.org/10.1002/jgrb.50179

Zhao, D., Kanamori, H., & Wiens, D.   (1997, March).   State of stress before and after the 1994 Northridge Earthquake. *Geophysical Research Letters*, *24*(5), 519–522.   Retrieved 2022-02-22, from `http://doi.wiley.com/10.1029/97GL00258`   doi: 10.1029/97GL00258

Zoback, M. D. (2000, May). Strength of the San Andreas. *Nature*, *405*(6782), 31–32.   Retrieved 2021-10-26, from `https://www.nature.com/articles/35011181/email/correspondent/c1/new`   doi: 10.1038/35011181

Zoback, M. D., & Healy, J. H.   (1992).   In situ stress measurements to 3.5 km depth in the Cajon Pass Scientific Research Borehole: Implications for the mechanics of crustal faulting.   *Journal of Geophysical Research: Solid Earth*, *97*(B4), 5039–5057.   Retrieved 2021-09-21, from `https://onlinelibrary.wiley.com/doi/abs/10.1029/91JB02175`   (_eprint: https://agupubs.onlinelibrary.wiley.com/doi/pdf/10.1029/91JB02175)   doi: 10.1029/91JB02175